Sparse norm and Cross-gradient inversions of gravity and magnetic data sets utilizing open-source resources in Python (Case study: Hematite ore body in Jalal Abad area (Iran))

E. Ardestani, V.[1] ✉ iD

1. Department of Earth Physics, Institute of Geophysics, University of Tehran, Tehran, Iran.

Corresponding Author E-mail: ebrahimz@ut.ac.ir

Abstract

The gravity and the magnetic data sets are utilized to model the Hematite ore body. The cross-gradient joint inversion is used to invert the data sets simultaneously. To discretize the model space, the advanced meshing algorithm (Octree mesh) has been applied. The sparse norm and cross-gradient inversion modules in Python, accessible through Simulation and Parameter Estimation in Geophysics (SimPEG, version 0.17.0) website, have been applied to the inversion process. The sparse norm inversions do not provide reasonable results, particularly for the gravity data set. The estimated density contrasts through the inversion process are very low and unrealistic and on the other hand, the north-south cross sections do not represent a real image from the subsurface sources. The magnetic modeling results obtained through sparse norm inversion also show unrealistic characters, particularly for the 3-dimensional figure of the subsurface anomaly.

The cross-gradient inversion acts quite successfully for both gravity and magnetic models in spite of high noise level in gravity data and the weak signal of magnetic data. The results are in good agreement with geological evidences and also former geophysical survey in the survey area. The priority of cross-gradient inversion of gravity and magnetic data sets to separate inversion is quite clear, despite the weak magnetic signal.

Keywords: Sparse norm inversion, Cross-gradient inversion, Gravity and magnetic data sets, Hematite ore-body.

1. Introduction

The inherent ambiguity in the inversion of individual data sets, especially potential field data, could be reduced considerably in a joint inversion utilization. The cross-gradient constraint (Gallardo, 2004), widely used in joint inversion methods, will lead to structurally similar subsurface models.

Some joint inversion methods are based on different physical property models with similar spatial distribution structures, such as cross-gradient joint inversion [e.g., Gallardo and Meju, 2004, Zhou, et al., 2015].

Gravity and magnetic data inversions have resulted in non-similar density and magnetization models. On the other hand, the proposed cross-gradient joint inversion algorithm have led to structurally similar models.

2. Geological setting

The survey area is located close to Zarand in Kerman province in Iran. The dominant host rocks in the area are igneous rocks of the Rizo formation. There are several volcano clastic dikes and sills intrusions in the area. Iron deposits are deep and have NW-SE strikes. Oxidation of iron ore bodies generates Hematite that is concentrated in shallow faults and cracks. The geological map showing the survey area is depicted in Figure 1 (Jolidehsar et al., 2021).

3. Input data

The Bouguer gravity data set and total intensity magnetic data are utilized for the joint inversion process. The magnetic measurements are carried out in a network with 20 m grid spacing between points and 40 m distance of profiles. The total intensity, inclination and declination are, 46600 nT, 48.2 degrees and 2.8 degrees, respectively. The gravity measurements are done at the same distances as the magnetic network. The Bouguer gravity anomalies and the residual total magnetic intensity are shown in Figures 2a and 2b, respectively.
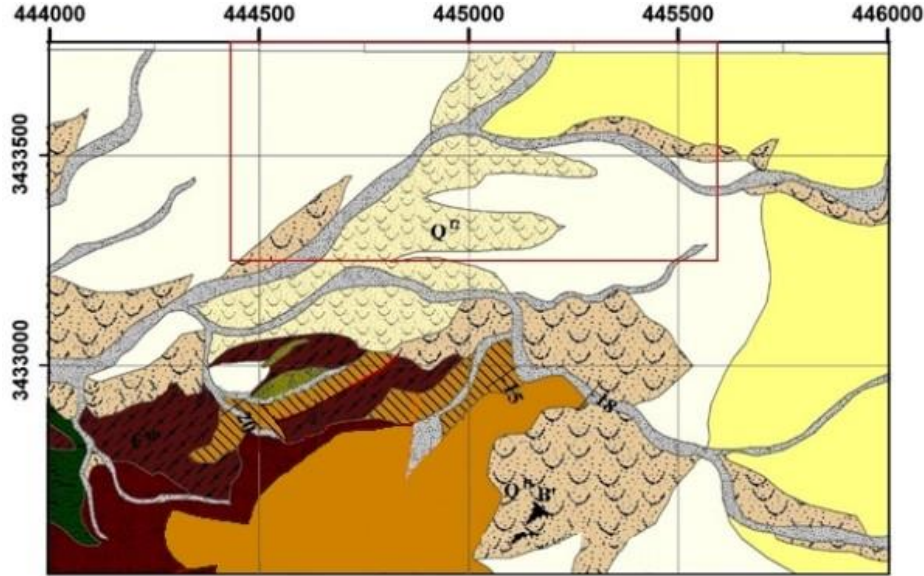
Figure 1. Q^{al}**:** Quaternary Deposits, Q^{r2}**,** Young windy sands, Q^{r1}**,** Old windy sands, Q^{tl}**,** Old trusts, ε^q**,** Quartzite, sandstone, phyllite, tuff, $P\varepsilon^q$**,** siltstone, sandstone tuff, $P\varepsilon^f$**,** Flysch stones (sandstone, shale, siltstone).

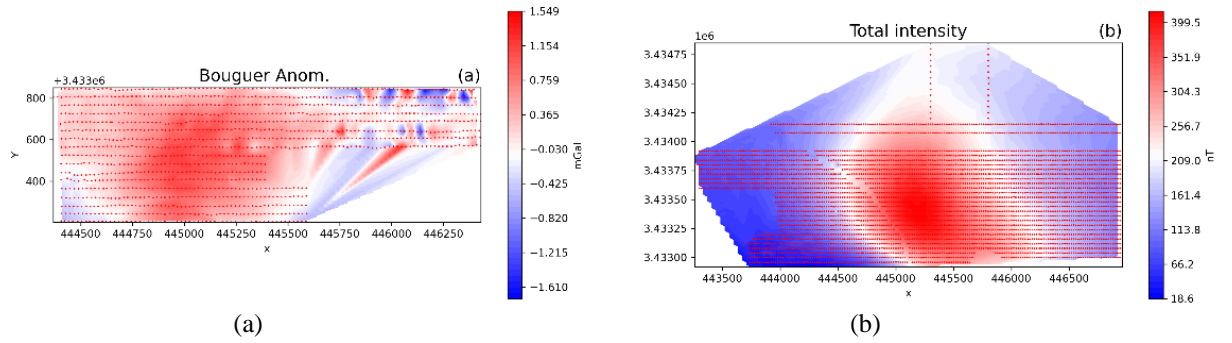(a)   (b)

Figure 2. a) Bouguer anomalies (mGal), b) Total magnetic intensity (nT).

4. Gravity data processing

Observed Bouguer gravity anomalies are shown in Figure 2a. Regional effects are first removed by using the polynomial fitting method. The Bouguer anomalies in Figure 2a have a strong trend in the northeast-southwest direction. This trend represents the regional anomalies and is simulated by a polynomial with degree 2. The coefficients of the polynomial are estimated through Scipy modules (Jones et al., 2001). The residual anomalies are computed by subtracting the regional effects from the Bouguer anomalies. The residual anomalies are depicted in Figure 3a.

Smoothing the anomalies and deleting near surface noises, the residual anomalies are upwarded to a height of 40 m, and the results are shown in Figure 3b. The 40 m height is selected due to the existence of quaternary deposits and conglomerates from the ground surface to a depth of 59 m in bore-hole drilling that will be shown in the next sections. The Fourier transform is applied to upward the residual anomalies,

$$G_z(p,q) = e^{-z\sqrt{p^2+q^2}} G_0(p,q) \qquad (1)$$

where $G_z(p,q)$ and $G_0(p,q)$ are 2-d discrete transform of data in height z and ground surface respectively and p, q are wave numbers of x and y, the coordinates of the gravity points.
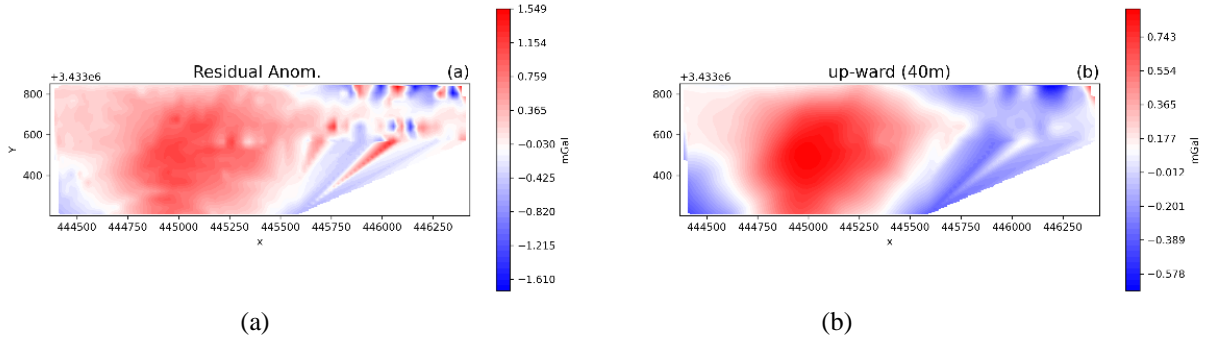
(a)   (b)

Figure 3. a) Residual gravity anomalies (mGal), b) up-warded gravity anomalies (mGal).

5. The sparse norm inversion method

In the first step, we invert gravity and magnetic data sets separately by applying the sparse inversion module accessible through SimPEG (Cockett et al., 2015). The theory of this method has been presented in detail in the authors' previous works (Ardestani et al., 2021).

The optimization problem is non-linear as β is not known. There are also imposed bounding constraints and using sparse norm. So it is solved utilizing a projected Gauss-Newton approach that employs a conjugate gradient solver (SimPEG).

Objective function in the L2 norm is written as follows (Oldenburg and Li, 2005):

$$\emptyset(\boldsymbol{m}) = \frac{1}{2}\|W_d(F(\boldsymbol{m}) - \boldsymbol{d}_{obs})\|_2^2 +$$
$$\frac{1}{2}\beta\|W_m(\boldsymbol{m} - \boldsymbol{m}_{ref})\|_2^2 \qquad (2)$$

Assuming that β is fixed, our goal is to find m that minimizes Equation (2). Using an iterative procedure and letting m^n be the current model and δm the perturbation, and expanding $\emptyset(\boldsymbol{m})$ in a Taylor series and ignoring the higher-order terms yields:

$$\emptyset(\boldsymbol{m^n} + \delta\boldsymbol{m}) = \emptyset(\boldsymbol{m^n}) + g^T\delta\boldsymbol{m} + \frac{1}{2}\delta_m^T H\delta m \qquad (3)$$

Taking the derivative of Equation (3) with respect to $\delta\boldsymbol{m}$ and setting the resultant equal to zero finally we have (Oldenburg and Li, 2005),

$$(J^T W_d^T W_d J + \beta W_m^T W_m)\delta\boldsymbol{m} =$$
$$J^T W_d^T W_d(\boldsymbol{d}_{obs} - F(\boldsymbol{m})) - \beta W_m^T W_m(\boldsymbol{m} - \boldsymbol{m}_{ref}) \qquad (4)$$

This is called the Gauss-Newton equation. Obtaining the $\delta\boldsymbol{m}$ through Equation (4) the updated model at the n+1 iteration is:

$$\boldsymbol{m^{n+1}} = \boldsymbol{m^n} + \delta\boldsymbol{m} \qquad (5)$$

The iteration continues until a solution with an acceptably small misfit is found.

6. Cross-gradient joint inversion

A key difficulty in the joint inversion of two or more seemingly disparate geophysical data sets is how to couple the model parameters. An efficient philosophy is the use of common geometrical constraints. A convenient un-normalized way to measure the geometrical similarity of the models is through the use of the cross-gradient function (Gallardo & Meju, 2004) given by:

$$\boldsymbol{\tau}(x, y, z) = \nabla\boldsymbol{m}_g(x, y, z) \times \nabla\boldsymbol{m}_T(x, y, z) \qquad (6)$$

where the null values of this function determine either the full collinearity or the negligibility of the gradients of the models ($\boldsymbol{m}_g \ and \ \boldsymbol{m}_m$) at corresponding positions and, therefore, can be used to constrain the models. While avoiding normalization of the cross gradients, we favor stable iterative search procedures for this second-order function (Gallardo & Meju, 2004) and encourage the dominance of the largest gradient, required by either data set, in saddle points. To discretize the model space, the 3-D model of the subsurface is discretized into a group of m rectangular blocks, each block (hereafter referred to as a cell) having a constant density and magnetization. The set of parameters is jointly estimated by defining an objective function that incorporates the following criteria

(i) Lowering criteria: The gravity and magnetic models should satisfactorily reproduce their respective predicted data in a least-squares sense by simultaneously minimizing,

$$\emptyset_g = \sum_{i=1}^{N}\left\{\frac{g_i^{obs} - g_i^{cal}}{\sigma_{gi}}\right\}^2 \qquad (7)$$

$$\emptyset_T = \sum_{i=1}^{N} \left\{ \frac{T_i^{obs} - T_i^{cal}}{\sigma_{Ti}} \right\}^2 \qquad (8)$$

where σ_{gi} and σ_{Ti} are standard deviations of the data errors.

(ii) The gravity and magnetic models should be structurally identical in terms of the cross-gradient function, that satisfy:

$$\tau_i = \nabla_i \boldsymbol{m_g} \times \nabla_i \boldsymbol{m_T} = 0, \; i = 1,..,N \qquad (9)$$

Gallardo (2004) showed that conditions (7) and (8) are not always sufficient to fully constrain gravity and magnetic models and that they are still dependent, to a great extent, on the coverage of geophysical data themselves. Because of this, areas covered by only one data set may yet find multiple models that equally satisfy the data and cross-gradient constraints (e.g. any constant or parallel image). Thus, the selection of any of such ambiguous solutions will still require a priori information. As a partial remedy to this problem, two regularizing conditions were implemented in the present development, as described below.

(iii) The models should be as simple as possible, providing they still justify their data and the cross-gradient constraint. This is achieved using smoothness (Tikhonov & Arsenin, 1977) and ridge regression-type constraints. This last constraint serves for maintaining closeness to an a priori model and it is particularly useful for assigning resistivity or velocity values in areas without data coverage or where directly sampled parameter values (e.g. from rock outcrop characterization or borehole logging) are available. The corresponding term of the objective function is:

$$\emptyset_{apr} = \sum_{i=1}^{N} \left[\alpha_g^2 \nabla_i^2 m_g + \alpha_T^2 \nabla_i^2 m_T + \right.$$
$$\left. \left(\frac{m_{gi} - m_{gi}^{apr}}{\sigma_{gi}^{apr}} \right)^2 + \left(\frac{m_{Ti} - m_{Ti}^{apr}}{\sigma_{Ti}^{apr}} \right)^2 \right] \qquad (10)$$

where α_g^2 and α_T^2 define the level of smoothness required in the models m_{gi}^{apr} and m_{Ti}^{apr} are the parameter values for any a priori gravity and magnetic models with standard deviations σ_{gi}^{apr} and σ_{Ti}^{apr} respectively. The composite objective function for the cross gradient joint inversion of gravity data is:

$$\min\{t = \emptyset_g + \emptyset_T + \emptyset_{apr}\}$$

Subject to $\tau_i = 0, \; i = 1,....,N$ \qquad (11)

This objective function can be solved iteratively using the non-linear functions involved in (2)–(5) (Green 1984).

The Gauss-Newton method is an effective method for minimizing an objective function iteratively. For moderately sized problems, the Gauss-Newton method typically converges much faster than gradient-descent methods.

By expanding the objective function in a Tylor series and assigning its first order and second order derivatives of it equal to zero, Equation (12) is obtained for updating the perturbation h,

$$[\boldsymbol{J^T W J}]\boldsymbol{h_n} = \boldsymbol{J^T W}(\boldsymbol{d^{obs}} - \boldsymbol{d^{pred}}) \qquad (12)$$

where W is a diagonal matrix whose elements are equal to

$$w_{dii} = 1/\sigma_i \qquad (13)$$

and σ_i is an estimated standard deviation of the ith datum that has three elements, $w = (w_g, w_T, w_t)$

J is the Jacobian matrix and $(\boldsymbol{d^{obs}} - \boldsymbol{d^{pred}})$ is a sum of the gravity and magnetic misfit functions.

$$\emptyset_d = \left(\boldsymbol{d_g^{obs}} - \boldsymbol{d_g^{pred}} \right) + \left(\boldsymbol{d_T^{obs}} - \boldsymbol{d_T^{pred}} \right) \qquad (14)$$

Obtaining the perturbation h_n, the iteration procedure continues as follows:

$$\boldsymbol{m^{n+1}} = \boldsymbol{m^n} + \boldsymbol{h_n} \qquad (15)$$

7. Forward equations

To compute the misfit functions in cross-gradient joint inversion, the gravity and magnetic forward equations should be used to simulate the gravity and magnetic data set.

7-1. Gravity forward equation

The model space is parametrized by an octree mesh (Haber & Helmann, 2007) and then the predicted data would be the sum of the gravity effects of the cells in each gravity point on the ground surface,

$$F(\boldsymbol{m}) = \boldsymbol{d}_{pred} \qquad (16)$$

The gravity effect of each cell of the octree mesh is computed by applying the equation presented by Pluff (1976),

$$F(m) =$$
$$G\rho \sum_{i=1}^{2} \sum_{j=1}^{2} \sum_{k=1}^{2} \mu_{ijk} \left[z_k \arctan \frac{x_i \; y_j}{z_k \; R_{ijk}} - \right.$$

$$x_i \log(R_{ijk} + y_i) - y_j \log(R_{ijk} + x_i) \Big] \qquad (17)$$

where

$$R_{ijk} = \sqrt{x_i^2 + y_j^2 + z_k^2} \qquad (18)$$

and

$$\mu_{ijk} = (-1)^i (-1)^j (-1)^k \qquad (19)$$

where G is the universal gravitational constant and ρ is the density.

7-2. Magnetic forward equation

From the related literature, the magnetization M and magnetic induction B are connected by the following equation:

$$\boldsymbol{B}(\boldsymbol{R}) = \frac{\mu_0}{4\pi} \nabla \int \boldsymbol{M}(\boldsymbol{R_0}) \cdot \nabla_0 \frac{1}{|R - R_0|} dV_0 \qquad (20)$$

where μ_0 is the permeability of the free space and R and R_0 are the observation and source locations, respectively. The unit of magnetization is the Ampere/meter, although this is seldom used in geophysics and the unit of magnetic induction is in Tesla, which turns out to be a very large quantity compared to anything which is measured in geophysics. For that reason, magnetic measurements are almost invariably reported in nanoTeslas, abbreviated nT. Nearly all magnetometers in use today measure the total magnetic intensity T, which is just the magnitude of the magnetic induction: T = |B|. The magnetic induction in turn can be considered as being composed of the ambient earth's field $\mathbf{B}_0$ and a component $\Delta\mathbf{B}$ due to the magnetic material in the subsurface. Generally, but not always, $\Delta\mathbf{B}$ is much smaller than $\mathbf{B}_0$, so we can approximate to first order in $\Delta\mathbf{B}/\mathbf{B}_0$:

$$\boldsymbol{T} \cong |\boldsymbol{B}_0| + \frac{\boldsymbol{B_0}}{|\boldsymbol{B_0}|} \cdot \Delta\boldsymbol{B} = T_0 + \Delta T \qquad (21)$$

where T_0 is the normal total magnetic intensity and ΔT is the anomalous total magnetic intensity. The anomalous total magnetic intensity of a rectangular prism is computed through Equation (22) (Rao and Babu 1991),

$$\Delta T = \sum_{i=1}^{2}\sum_{j=1}^{2}\sum_{k=1}^{2} \mu_{ijk} G_1 \ln(R_{ijk} + x_i) + G_2 \ln(R_{ijk} + y_j) + G_3 \ln(R_{ijk} + z_k) + G_4 \arctan\frac{x_i z_k}{R_{ijk} y_j} + G_5 \arctan\frac{y_j z_k}{R_{ijk} x_i} \qquad (22)$$

where $G_1 = EI(Mr + Nq)$, $G_2 = EI(Lr + Np)$, $G_3 = EI(Lq + Mp)$, $G_4 = EI(Nr - Mq)$, $G_5 = EI(Nr - Lp)$, EI is magnetic susceptibility, r, q and p are the cosine directions of the magnetic field and L, M, N is the cosine directions of magnetization.

8. Inversion results

The up-warded residual gravity anomalies in Figure 3b are inverted through sparse norm inversion, and the cross-sections of the inversion results are shown in Figures 4a - 4c and 5a - 5c. The observed and predicted gravity and the difference (misfit) are depicted in Figures 6a - 6c, respectively. As it is clear, the normalized misfits are absolutely unacceptable.

The residual total magnetic anomalies are also inverted and the cross sections of the results are shown in Figures 7a - 7c and 8a - 8c. The observed predicted and misfit values of magnetic anomalies are depicted in Figures 9a - 9c.

The cross-sections of the magnetic inversion through the cross-gradient method are shown in Figures 12a – 12c and 13a – 13c.
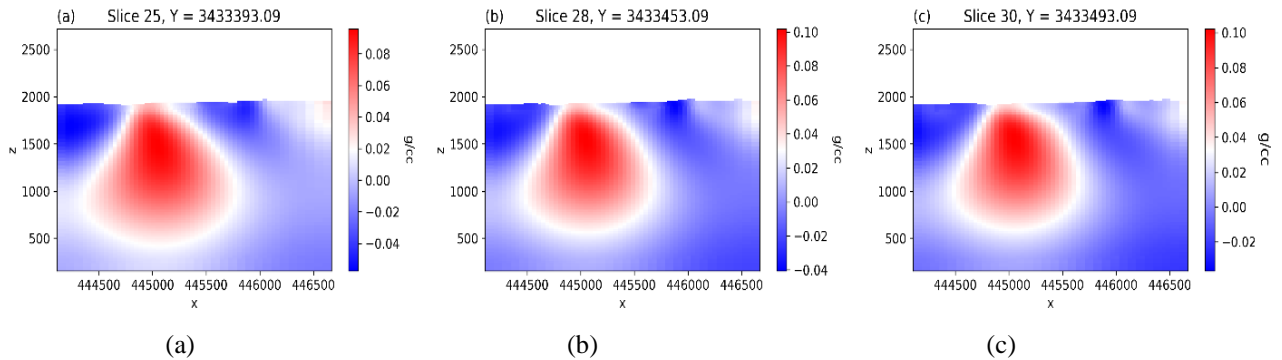

Figure 4. a), b), c), Y slices of density contrast (g/cc) obtained through sparse norm inversion.
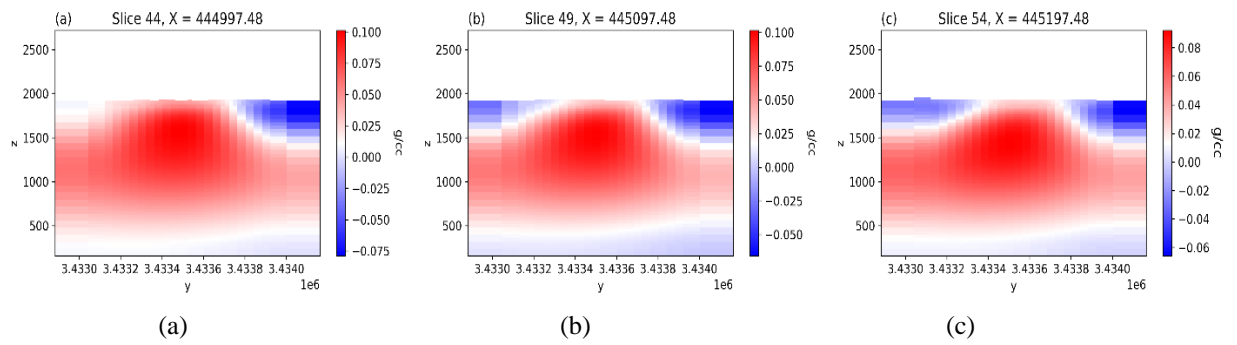
Figure 5. a), b), c), X slices of density contrast (g/cc) obtained through sparse norm inversion.
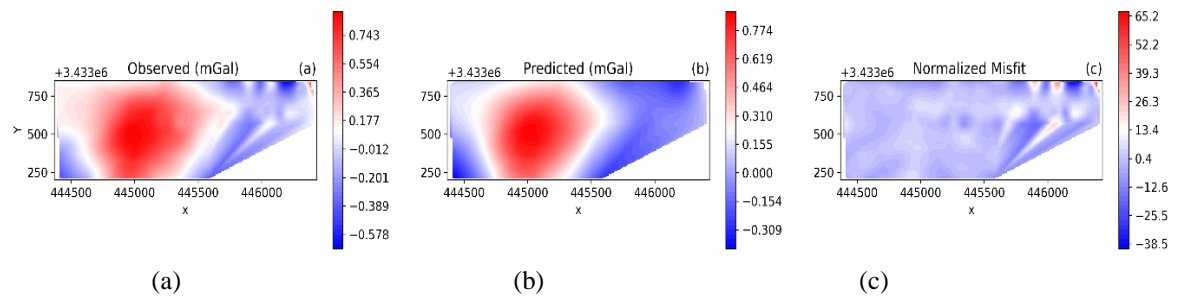

Figure 6. a) The observed gravity anomalies (mGal), b) The calculated gravity anomalies (mGal), c) The normalized misfit between observed and calculated anomalies.
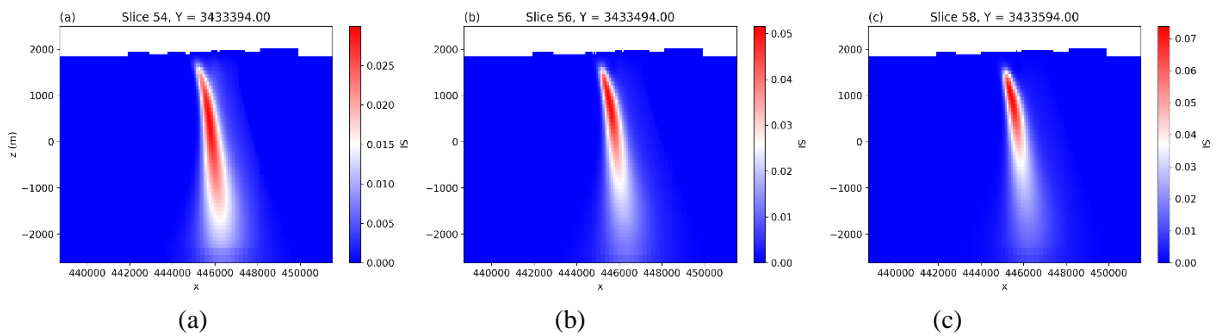

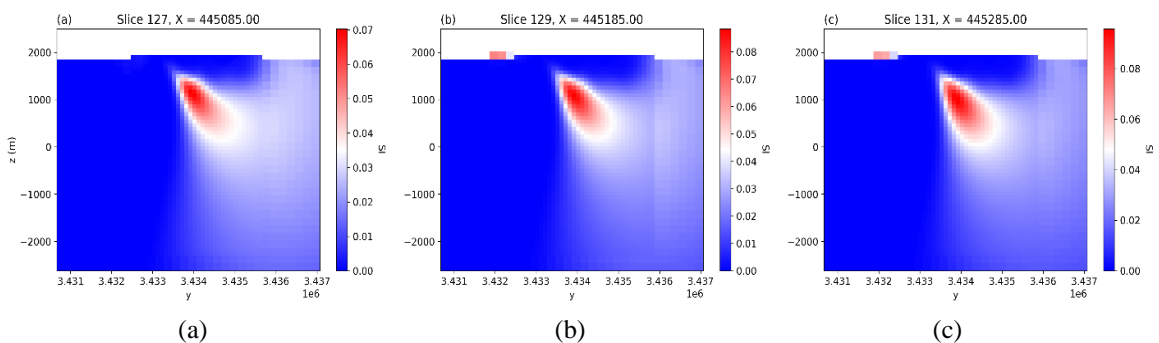**Figure 7.** a), b), c) Y slices of susceptibility (SI) obtained through sparse norm inversion.

Figure 8. a), b), c) X slices of susceptibility (SI) obtained through sparse norm inversion.

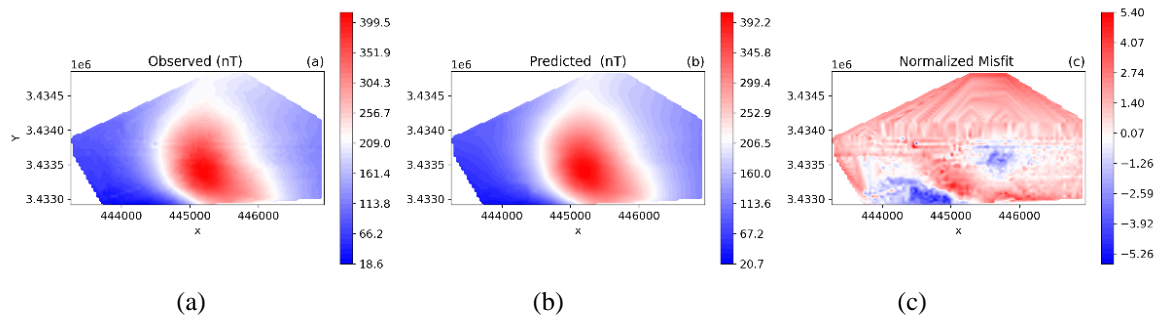(a)   (b)   (c)

Figure 9. a) The observed magnetic anomalies (nT), b) The calculated magnetic anomalies (nT), c) The normalized misfit between observed and calculated anomalies.
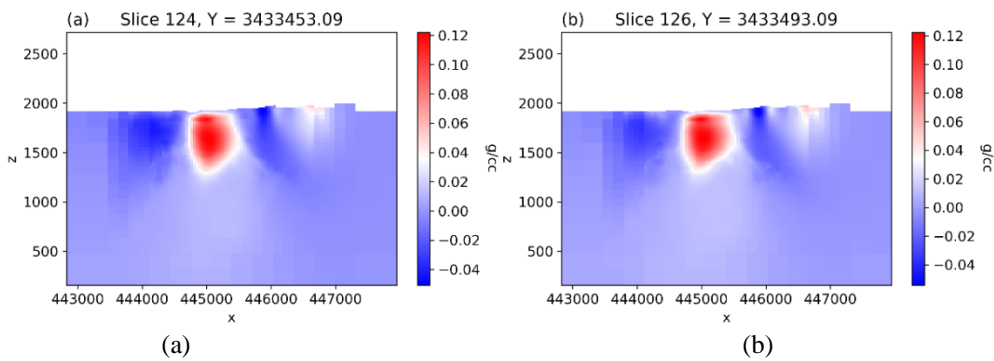

(a)   (b)

Figure 10. a), b) Y slices of density contrasts (g/cc) obtained through cross-gradient inversion.
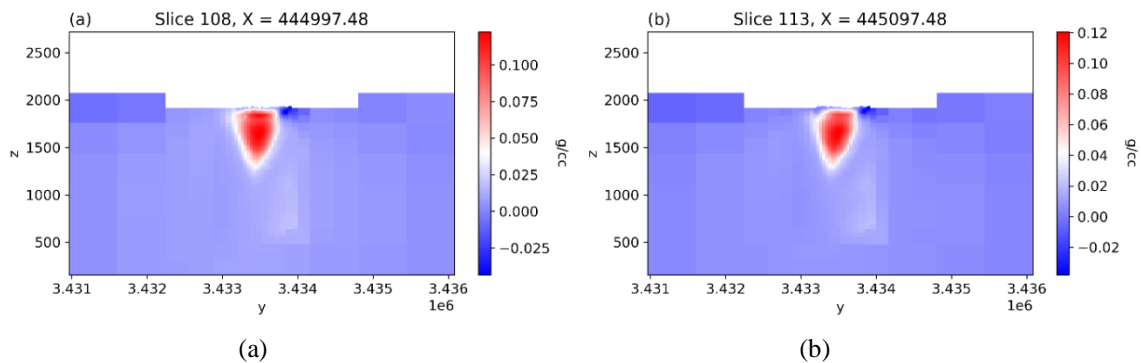

(a)   (b)

Figure 11. a), b) X slices of density contrasts (g/cc) obtained through cross-gradient inversion.

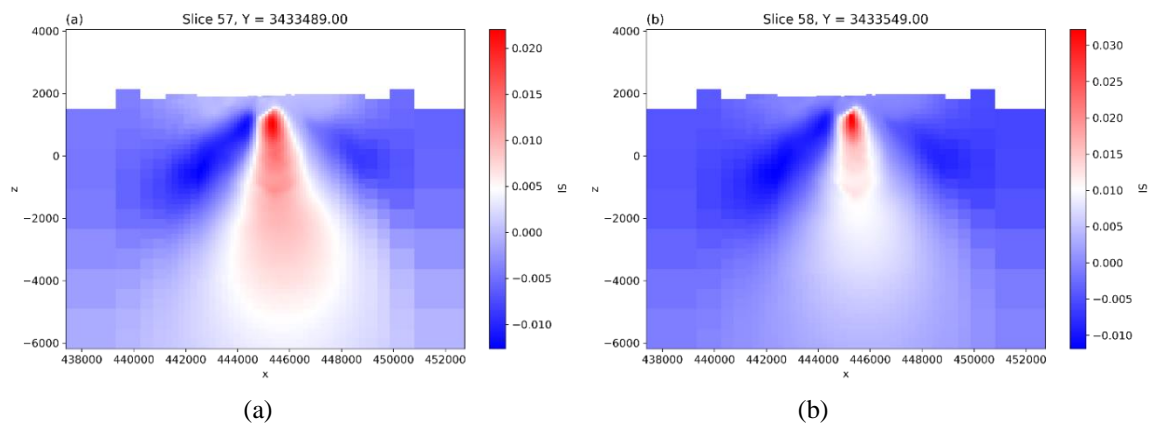(a)   (b)

Figure 12. a), b) Y slices of susceptibility (SI) obtained through cross-gradient inversion.
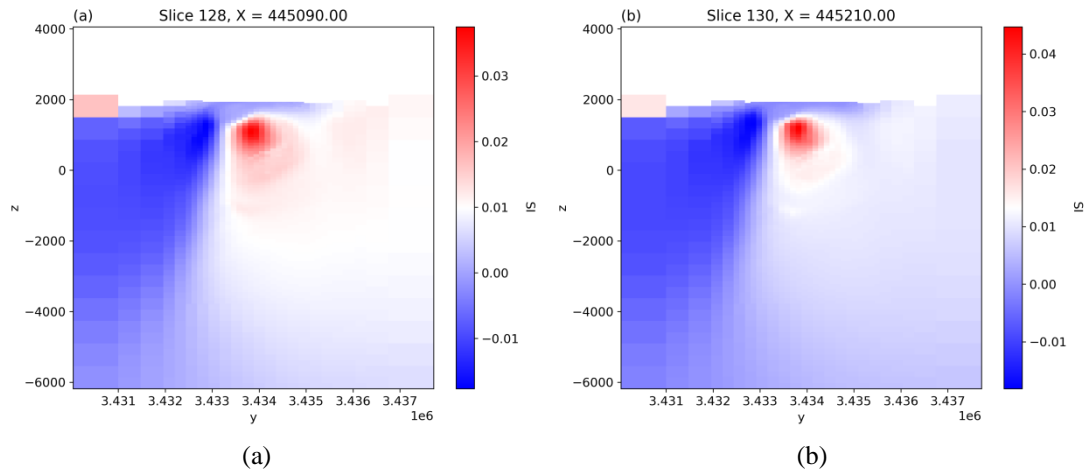
Figure 13. a), b) X slices of susceptibility (SI) obtained through cross-gradient inversion.

9. Discussion

The first report on inverting the gravity and magnetic report in the survey area is published by Jolidehsar et al. (2021). They assessed the inversion results by the detected rock formation accessible through a bore-hole in the area. The maximum depth of the bore-hole is about 420 m that can be used for gravity inversion results and not the magnetic ones.

The detected rocks in the bore-hole and their average density and magnetic susceptibility are shown in Table 1.

Due to the shortage of gravity observation points and the small size of the gravity network, the gravity sparse norm inversion results (Figures 4a – 4c and 5a – 5c) show unrealistic results with very low recovered density contrasts.

Magnetic sparse norm inversion results in y-cross sections (Figures 7a – 7c) demonstrate a dike-type character that extends to a depth of more than 2000 m, which is unlikely to be correct. The x-cross sections (Figures 8a –

8c) are more reasonable considering the former geological and geophysical investigations.

The gravity inversion results through the cross-gradient method (Figures 10a – 10b and 11a – 11b) show the existence of the anomaly from a very shallow depth to about 400 m depth which is very close to the maximum depth of high-density dolomite (367 m) in the bore-hole.

The magnetic inversion results through the cross-gradient method (Figures 12a – 12b and 13a – 13b) are also quite informative and reasonable despite the weak magnetic signal.

Considering the average height of the ground surface which is about 1900 m, all cross-sections show that the subsurface magnetic anomaly begins from 400 m depth from the ground surface and extends to the 900 m depth.

The dolomite with iron oxide detected in the bore-hole from 123 m to 367 m depth is not the cause of the magnetic anomaly and the magnetic source is much deeper.

Table 1. Bore-hole results.

Formation	Maximum depth of drilling (m)	Average Density (g/cm3)	Average Susceptibility $10^{-6}SI$
Quaternary deposits and conglomerate	59.2	2.4	
Dolomite	82	2.7	10
Sandstone	111	2.4	0-20
Dolomite	123	2.7	10
Dolomite with iron oxide	367	2.9	-
Shale	390	2.3	63
Sandstone	393	2.4	0-20
Dioritic Dike	395	2.9	630
Sandstone	397	2.4	0-20
Shale	409	2.3	63
Dolomite	420	2.7	10

10. Conclusions

The inverted gravity and magnetic data sets through sparse norm inversion provide weak results that are unrealistic. Applying the cross-gradient joint inversion provides much more reasonable and realistic results that are consistent with the geological and geophysical evidence in the survey area.

The inverted magnetic data through the cross-gradient method provides valuable results about the depth and geometrical shape of the causative body that is absolutely new and were not obtained by former geophysical research and magnetic inversion. A deep future bore-hole that reaches a depth of 1000 m can provide important information about the source of the magnetic anomaly.

References

Ardestani, V.E., Dominique, F., & Oldenburg, D. (2021). Gravity and Magnetic Processing and Inversion Over the Mahallat Geothermal System Using Open Source Resources in Python. *Pure and Applied Geophysics*, 178. doi:10.1007/s00024-021-02763-6.

Cockett, R., Kang, S., Heagy, L.J., Pidlisecky, A., & Oldenburg, D.W., (2015). SimPEG: an open source framework for simulation and gradient based parameter estimation in geophysical applications. Comput. Geosci. 85, 142–154. http://dx.doi.org/10.1016/j.cageo.2015.09.015. http://www.sciencedirect.com/science/article/pii/ S009830041530056X.

Gallardo, L.A. (2004). Joint two-dimensional inversion of geoelectromagnetic and seismic refraction data with cross-gradients constraint. University of Lancaster.

Gallardo, L.A., & Meju, M.A. (2004). Joint two-dimensional DC resistivity and seismic travel time inversion with cross-gradients constraints. *Journal of Geophysical Research: Solid Earth*, 109 (B3).

Green, P.J. (1984). Iteratively Reweighted Least Squares for Maximum Likelihood Estimation, and some Robust and Resistant Alternatives. *J. R. Statist. Soc.*, 46(2), 149-192.

Haber, E., & Heldmann, S. (2007). An octree multi grid method for quast-static Maxvell's equations with highly discontinuous coefficients. *J. Comput. Phy.*, 65, 324-337.

Jones, E., Oliphant, T., & Peterson, P. (2001). {SciPy}: open-source scientific tools for {Python}. URL ⟨http://www.scipy.org/⟩.

Jolidehsar, F., Moradzadeh A., & Dolati ardehjani, F. (2021). 3-D sparse joint inversion of cross-gradient using smoothness constraint for gravity and magnetic data sets of iron deposit of Jalal abad mine. *Journal of Mining Engineering (JME)*, 15(49), 67-88.

Oldenburg, D.W., & Li, Y. (2005). Inversion for Applied Geophysics: A Tutorial, pp. 89–150 (Chapter 5). URL ⟨http://library.seg.org/doi/abs/10.1190/1.9781560801719.ch5⟩.

Pluff, D. (1976). Gravity and Magnetic fields of polygonal prisms and application to magnetic terrain corrections. *Geophysics*, 41, 727-41.

Rao, D.B, & Babu, N.R. (1991). A rapid method for three-dimensional modeling of magnetic anomalies,. *Geophysics*, 56, 1729-37.

Tikhonov A.V., & Arsenin V.Y. (1977). Solution of ill-posed problems: John Wiley & Sons, Inc.

Zhou, J., Meng, X., Guo, L., & Zhang, S. (2015). Threedimensional cross-gradient joint inversion of gravity and normalized magnetic source strength data in the presence of remanent magnetization. *Journal of Applied Geophysics*, 119, 51-60.